# Journal of Materials Chemistry C

Accepted Manuscript


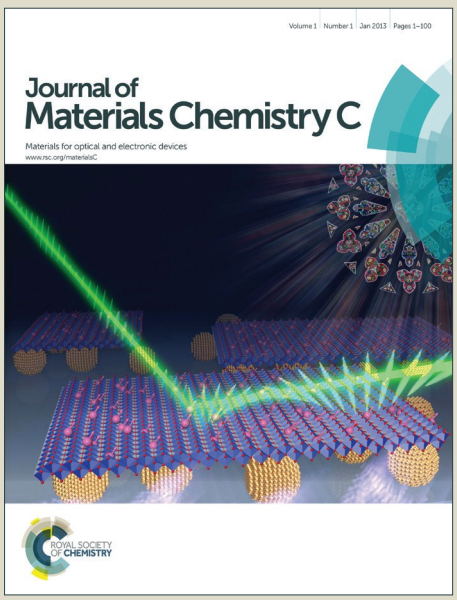





ROYAL SOCIETY OF CHEMISTRY

www.rsc.org/materialsC

# Effect of aliovalent doping on properties of perovskite-like multiferroic formates

Mirosław Mączka,*[,a] Adam Sieradzki,[b] Bartosz Bondzior,[a] Przemysław Dereń,[a] Jerzy Hanuza,[a] and Krzysztof Hermanowicz[a]

[†]*Institute of Low Temperature and Structure Research, Polish Academy of Sciences, Box 1410, 50-950 Wrocław 2, Poland*

[‡]*Faculty of Fundamental Problems of Technology, Wrocław University of Technology, Wybrzeże Wyspiańskiego 27, 50-370, Wrocław, Poland*

## ABSTRACT

We report synthesis, thermal, dielectric, Raman, IR and luminescence studies of chromium-doped multiferroic MOF, $[(CH_3)_2NH_2][Mn(HCOO)_3]$ (DMMn). These studies reveal that doping with chromium(III) leads to lowering of the ferroelectric phase transition temperature $T_c$. The doping also changes the character of the phase transition from strongly first-order for undoped sample to partially diffused one for 3.1% of chromium doping. This behavior resembles behavior of inorganic $ABO_3$ perovskite ferroelectrics where doping often leads to decrease of $T_c$ and diffuse character of a phase transition. We also show that the chromium-doped sample exhibits efficient luminescence. Additional studies demonstrated that $[(CH_3)_2NH_2][M^{II}(HCOO)_3]$ formates ($M^{II}$=Mg, Mn, Co) may also be doped with other trivalent cations such as $Al^{3+}$, $In^{3+}$, $Eu^{3+}$ or $Er^{3+}$.

Doping with these ions also leads to decrease of $T_c$ and diffuse character of the phase transition. Additional optical studies show that europium-doped DMMn sample also exhibit luminescent properties. Thus our discovery opens up a new and simple route for synthesis of various multifunctional amine-templated metal formate frameworks with tunable multiferroic and luminescent properties by doping these frameworks with wide range of trivalent cations.

## Introduction

Ferroelectric materials have found many technological applications and $ABO_3$ oxides crystallizing in perovskite architecture constitute one of the most important family of ferroelectrics.[1] Properties of these oxides may be tailored by doping at A- and/or B-sites by both isovalent and aliovalent cations.[1,2] In particular, doping generally leads to shift of the phase transition temperature and the phase transition may become diffuse.[1,2] When doping is sufficiently large, a microscopic phase transition may no longer be observed and the material may exhibit strong dielectric relaxation attributed to presence of polar nanoregions.[1,2] Relaxor ferroelectrics have received a lot of attention due to their excellent electro-mechanical properties, among others.[1] Although ferroelectrics are widely used in various technological applications, there is growing demand for discovery of novel materials possessing two or more useful properties in one phase. Multiferroics constitute one of such group of multifunctional materials. Most interesting are those, which exhibit coexistence of both electric and magnetic orders since such materials are promising for application in data storage media, electromagnetic sensors, telecommunication systems etc.[3] One of the most extensively studied multiferroic material crystallizing in a perovskite architecture is $BiFeO_3$ and its properties may be strongly modified by doping.[3]

In recent years, synthesis of metal-organic frameworks (MOFs) was shown to be novel and very promising way for obtaining multiferroic materials.[4] Multiferroic properties were confirmed for [cat][$M^{II}(HCOO)_3$], where cat= dimethylammonium ($DMA^+$) or $NH_4^+$ cation, and M=Mn, Co, Ni or Fe.[4-6] It was also suggested that coexistence of electric and magnetic order exists in imidazolium manganese formate [$C_3N_2H_5$][$Mn(HCOO)_3$], hydrazinium metal formates [$NH_2NH_3$][$M^{II}(HCOO)_3$] with M=Mn, Co, guanidinium copper formate [$C(NH_2)_3$][$Cu(HCOO)_3$] and ethylammonium metal formates [$CH_3CH_2NH_3$][$M(HCOO)_3$] with M=Mg, Mn.[7] It is worth noting that recent report showed that magnetoelectric coupling in DMMn may be observed already in the paramagnetic phase.[8] Since discovery of these multiferroics, numerous attempts were undertaken to synthesize other perovskite multiferroics by using different organic cations such as azetidinium, hydroxylammonium and formamidinium.[9-12] Although many new compound have been discovered, which posses interesting magnetic and dielectric properties, ferroelectric properties were not confirmed in any of these compounds.[9-12] A second possible way for obtaining novel organic multiferroics is preparation of compounds containing frameworks built up of different metal cations. This route was successfully employed for synthesis of [$(CH_3)_2NH_2$][$Fe^{III}M^{II}(HCOO)_6$] compounds ($M^{II}$=Fe, Mn, Co, Mg, Ni, Zn, Cu) that crystallize in niccolite architecture,[13-16] and [$(CH_3)_2NH_2$][$Na_{0.5}M^{III}_{.0.5}(HCOO)_3$] frameworks ($M^{III}$=Cr, Fe) crystallizing in the perovskite structure.[17,18] In this family of heterometallic compounds, coexistence of electric and magnetic order was observed only in the mixed-valence [$(CH_3)_2NH_2$][$Fe^{III}Fe^{II}(HCOO)_6$].[14,15]

Herein, we explore a third possibility for tailoring properties of amine-templated metal formates, i.e., doping with trivalent cations. This novel approach has not been yet explored in multiferroic MOFs but it is clear that doping opens the opportunity to play with the framework flexibility, which in turn should modify properties of the doped materials. We will show that the

doping with trivalent cations modifies properties and phase transition mechanism of the three studied here MOFs. It is also worth adding that doping may allow obtaining novel luminescent materials by selecting appropriate MOFs and lanthanide or other cations. We will show in the present report that doping adds new functionality to the studied here multiferroic MOFs, i.e., these compounds may be doped with chromium or lanthanide ions that make them promising luminescent materials.

## Experimental

### Synthesis

All reagents (analytically grade) used for synthesis are commercially available and used without further purification. All crystals were prepared under solvothermal conditions at 140 °C. In order to synthesize chromium-doped DMMn, a mixture of $MnSO_4 \cdot H_2O$ (1.96 mmol), $Cr(NO_3)_3 \cdot 9H_2O$ (0.04 mmol), DMF (30 mL) and $H_2O$ (30 mL) was heated in a Teflon-lined microwave autoclave for 24 hours. Block light green crystals were obtained by evaporating the solution at room temperature for 1 week. The crystals were filtered from the mother liquid and washed by ethanol. The remaining crystals of Co and Mg analogues were prepared in the same way by using $MgCl_2$ and $CoCl_2$ salts. We have also synthesized some crystals containing smaller concentration of $Cr^{3+}$ using the reaction mixture containing only 0.02 mmol of $Cr(NO_3)_3 \cdot 9H_2O$. For doping with $Al^{3+}$, $Eu^{3+}$, $Er^{3+}$ and $In^{3+}$, $Al(NO_3)_3 \cdot 9H_2O$, $Eu(NO_3)_3$, $ErCl_3 \cdot 6H_2O$ and $InCl_3$ salts were used. The phase purity of bulk samples was confirmed by a good match of their powder XRD patterns with the simulated ones based on the single crystal structures of pure DMMn, DMCo and DMMg (Figure S1, Supporting Information). The content of metal elements was determined by inductively

coupled plasma method (ICP), which was performed on an ARL 3410 ICP instrument. The concentrations of trivalent ions is given in Table S1.

**X-ray powder diffraction**

Powder XRD patterns were obtained for all samples on an X'Pert PRO X-ray diffraction system equipped with a PIXcel ultrafast line detector, focusing mirror, and Soller slits for $CuK\alpha_1$ radiation ($\lambda$=1.54056 Å).

**Heat Capacity**

Heat capacity was measured using Mettler Toledo DSC-1 calorimeter with high resolution of 0.4 μW. Nitrogen was used as a purging gas. The heating and cooling rate was 5 K/min. The excess heat capacity values associated with the phase transitions were evaluated by subtraction from the data the baselines representing variations in the absence of the phase transitions.

**Dielectric Properties**

The dielectric measurements at ambient pressure were carried out using a Novocontrol Alpha impedance analyzer (10mHz - 1MHz). Since the obtained single crystals were not big enough to perform single crystal dielectric measurements, pellet made of well-dried DMMn: 3.1% $Cr^{3+}$ sample was measured instead. The pellet was placed between two copper, flat electrodes of the capacitor with a gap of 0.5 mm. The small signal of an amplitude 1V was applied across the sample. The temperature was controlled by the Novo-Control Quattro system, with use of a nitrogen gas cryostat. The measurements were taken every 1 deg over the temperature range from 130 to 250 K. Temperature stability of the samples was better than 0.1 K.

### Raman and IR studies

Temperature-dependent IR study was performed for the DMMn: 3.1% $Cr^{3+}$ sample using Biorad 575C FT-IR spectrometer and a helium-flow Oxford cryostat. KBr pellet was used for the range of 3500-400 $cm^{-1}$ and Apiezon N suspension for the range of 500-50 $cm^{-1}$. The spectral resolution was 2 $cm^{-1}$. Raman spectra were measured using a Bruker FT 100/S spectrometer with YAG:Nd laser excitation (1064 nm) and a helium-flow Oxford cryostat.

### Optical studies

For measurements of $Cr^{3+}$ emission Varian Model 2300 Spectrophotometer along with Oxford Model CF 1204 continuous flow liquid helium cryostat equipped with temperature controller were used. Sample was excited with 450 nm RN-N Blue laser model. For measurements of excitation spectrum of the chromium-doped DMMn at 77 K, Xe lamp and McPherson optical measurement system with Hamamatsu R928 photomultiplier as a detector were used. Temperature of 77 K was obtained using liquid nitrogen and a Dewar flask. To measure decay profiles Continuum OPO Surelite I pumped with Nd:YAG laser as the excitation source and digital oscilloscope Tektronix model TDS 3052 were used. Electron reflectance spectra of europium and erbium-doped DMMn were measured using a Cary 5E spectrophotometer with the Praying Mantis diffuse reflectance accessory. Emission spectrum of europium-doped DMMn sample was measured using Hamamatsu photonic multichannel analyzer PMA-12 equipped with BT-CCD linear image sensor and Nd:YAG laser with Ti-sapphire converter as the excitation source.

## Results and discussion

**Thermal Properties**

The DSC measurements of DMMn, DMCo and DMMg show sharp heat anomalies characteristic for first-order phase transitions at 190, 159 and 265 K upon warming and 182, 149 and 259 K upon cooling, respectively (Figures S2-S5). The transition temperatures are in good agreement with those reported in literature.[19-23] The changes in heat capacity and entropy related to the phase transitions are presented in Figures 1 and S3-S5. The calculated changes in enthalpy $\Delta H$ and entropy $\Delta S$ of the studied compounds are listed in Table S1. The $\Delta S$ values obtained for DMMn (4.7 $Jmol^{-1}K^{-1}$) and DMMg (5.9 $Jmol^{-1}K^{-1}$) are close to the 4.6 $Jmol^{-1}K^{-1}$ value reported for DMMg.[21] The change in entropy for DMCo is smaller (3.4 $Jmol^{-1}K^{-1}$) when compared to DMMg and DMMn (Table S1). Figures 1, S2, S5 and S6 show that doping with $Cr^{3+}$ has significant impact on the phase transitions in DMMn and DMCo. Firstly, doping leads to pronounced lowering of $T_c$ (Table S1 and Figure S6). Secondly, the DSC and $\Delta C_p$ peaks become much broader and strongly asymmetric. Thirdly, changes in the transition entropies become less steep and smaller. It is worth noting that shift of $T_c$, broadening and asymmetry of thermal anomalies, and decrease of the transition entropy increase with increasing concentration of $Cr^{3+}$ ions. Very similar features were reported for many inorganic perovskites, for which shift of $T_c$, broadening of thermal anomalies and decrease of the entropy also increased with increasing concentration of doping ions (diffuseness of the phase transition).[1,2,24] Thus the observed features of the thermal anomalies for the chromium-doped DMMn and DMCo prove that $Cr^{3+}$ is incorporated into their frameworks, and doping changes the character of the phase transition from strongly first-order to diffused one. Chromium-doped DMMg samples show weaker effect, with $T_c$ shift of about 10 K for 2.2 % $Cr^{3+}$ doping, compared to 13 K shift for DMMn: 2.1 % $Cr^{3+}$ (see Table S1). Moreover, this compound does not show any significant change in the transition entropy upon doping. We

suppose that this behavior can be attributed to different stability and stiffness of the magnesium formate framework when compared to the Mn and Co analogues. Indeed, previous studies showed that Mg compound exhibits unusually high $T_c$ among the DMM compounds.[21]

In order to check if doping with other trivalent cations is also possible, we have performed synthesis of DMMn in the presence of $Al^{3+}$, $In^{3+}$, $Eu^{3+}$ and $Er^{3+}$. Our data show that effect of $Al^{3+}$ and $In^{3+}$ doping on $T_c$ is comparable to the effect of $Cr^{3+}$ doping (see Figure 1). Effect of $Er^{3+}$ doping is also strong, even stronger than $Cr^{3+}$ doping (Figure S6). $Eu^{3+}$ ions may also be incorporated into the DMMn matrix but in this case we were not able to obtain sample with only one thermal anomaly. Double DSC peak for this sample indicates that the grown DMMn: $Eu^{3+}$ sample is non-equilibrium material.[25]



Figure 1. (a) The change in heat capacity and (b) entropy related to the phase transition in DMMn, DMMn: 2.1 % $Cr^{3+}$, DMMn: 3.1% $Cr^{3+}$, DMMn: 2.0 % $Al^{3+}$ and DMMn: 3.5 % $In^{3+}$ measured in heating modes.

**Dielectric Properties**

Since DSC studies revealed that doping with aliovalent cations has significant impact on character of the phase transitions in the studied MOFs, we decided to perform detailed studies for

DMMn: 3.1% $Cr^{3+}$ as a representative sample. Figure 2 shows the real and imaginary components of the dielectric permittivity as a function of temperature for DMMn: 3.1% $Cr^{3+}$ for heating process. The results show an increase of temperature corresponding to the maximum value of the real part of dielectric permittivity $T_{max}$ with increasing frequencies. Nevertheless, the real part of the permittivity ε' is largely independent of frequency above $T_{max}$. Such a behavior implies the relaxor character of the investigated material. At the same time, the imaginary part of dielectric permittivity exhibits a broad frequency dependent peak. At first glance, both the imaginary and real part of dielectric permittivity graphs show a diffuse phase transition with no distinct anomalies owing to structural phase transitions. However, more detailed analysis revealed characteristic temperature of about 164 K, where the amplitude of the ε"(T) broad peak starts to decrease with decreasing frequency.



Figure 2. (a) Real and (b) imaginary dielectric permittivity responses as a function of temperature in DMMn: 3.1% $Cr^{3+}$. The representative curves are plotted in frequency decades between 0.1 Hz and 2 MHz. Dash line corresponds to the structural phase transition temperature.

Figure 3. Complex dielectric permittivity spectra of DMMn: 3.1% $Cr^{3+}$ (real part (a) imaginary (b)) at ambient pressure in temperature ranges indicated in the figures.

In Figure 3 dielectric response of the studied DMMn: 3.1% $Cr^{3+}$ sample is presented. It follows from the plot (Figure 3b) that for the investigated compound imaginary part of dielectric permittivity exhibits two relaxation peaks characteristic for dipolar relaxation, shifted towards lower frequencies with decreasing temperature. The first relaxation peak corresponds to the structural relaxation above the phase transition temperature and its temperature dependent shape may indicate that the effective relaxation response of the sample is contributed by more two relaxation processes. Second peak appears below the phase transition temperature. The dielectric loss spectra for the dominating peak deviate from the classical Debye behavior. The studied material reveals the anomalous, two-power-law relaxation mechanism represented by low- and high-frequency power-law dependence of the imaginary part of dielectric permittivity on frequency, i.e.:

$$\varepsilon''(f) \propto (f/f_{max})^{m} \quad \text{for } f < f_{max},$$
$$\varepsilon''(f) \propto (f/f_{max})^{n-1} \quad \text{for } f > f_{max},$$

where $f_{max}$ denotes the loss peak frequency and the power-law exponents fall in the range of $0 < m, n < 1$. Such a relaxation pattern was found to be characteristic also for related MOFs.[15,17] The temperature dependence of the power law exponents corresponding to the dominating relaxation peak is presented on Figure 4. At phase transition temperature the character of changes of both parameters can be noticed, which is attributed to the structural phase transition.



Figure 4. Temperature dependence of the power-law exponents in relaxation response of DMMn: 3.1% $Cr^{3+}$.

**Vibrational Studies**

In order to obtain further insight into structural changes and mechanism of the phase transition in DMMn: 3.1% $Cr^{3+}$, we employed Raman and IR methods since it is well known that vibrational methods are very sensitive to local distortion, defects and order-disorder phenomena.[26,27] Temperature-dependent Raman and polycrystalline IR spectra of DMMn: 3.1% $Cr^{3+}$ are presented in Figures S7-S9, Supporting Information, and Figures 5 and 6. The obtained results show that vibrational spectra of DMMn: 3.1% $Cr^{3+}$ are very similar to those reported for pure DMMn (Figures 5 and 6, and ref. 20). Upon cooling down to 160 K, the observed bands exhibit weak narrowing and shifts. Significant changes in the spectra become, however, evident below

160 K. Firstly, many bands exhibit significant narrowing. This behavior is especially pronounced for the $\rho(NH_2)$ IR mode observed near 920 $cm^{-1}$ (Figure 6(b)) and the lattice modes (Figure S7). Secondly, new bands appear and some bands split. For instance, the $\nu_3(HCOO^-)$ IR mode near 795 $cm^{-1}$ and the $\nu_5(HCOO^-)$ mode near 1370 $cm^{-1}$ split into doublets (Figure 6a and 6c). Third, some bands exhibit significant changes in intensity. This behavior is very clearly observed, for instance, for the Raman bands in the range 2800-2900 $cm^{-1}$ (Figure 5a).

Figure 5. (a) Detail of the Raman spectra results corresponding to the spectral range 3100-2750 $cm^{-1}$ for DMMn: 3.1% $Cr^{3+}$. For the comparison sake, data for previously reported DMMn are presented in (b).[18] Arrows indicate the bands that exhibit pronounced increase in intensity below the phase transition temperature.

Figure 6. Detail of the IR spectra results for DMMn: 3.1% $Cr^{3+}$ ((a), (b) and (c)) and undoped DMMn ((d), (e) and (f).

In order to better observe the temperature-dependent changes in the spectra, we show temperature evolution of a few selected vibrational frequencies and full widths at half maximum (FWHM) values for different molecular subunits of the studied compound (Figures 7, 8 and S10). These figures show very clear changes in frequency near the structural phase transition temperature. Since the observed frequency shifts are observed both for the $DMA^+$ and formate modes, the phase transition is related to distortion of both organic cation and manganese formate framework. Figure 8b also shows that the most significant changes in FWHM values are observed for the $\rho(NH_2)$ mode and this behavior proves that the phase transition in DMMn: 3.1% $Cr^{3+}$ is associated with ordering of $DMA^+$ cations.

Figure 7. Temperature evolution of (a) $\nu_{as}$(CNC) and (b) $\nu_{s}$(CNC) mode IR frequencies for DMMn: 3.1% $Cr^{3+}$ (circles) and DMMn (triangles). (c) FWHM of the $\nu_{as}$(CNC) bands for DMMn: 3.1% $Cr^{3+}$ (circles) and DMMn (triangles). Solid lines are to guide the eye.



Figure 8. Temperature evolution of (a) $\rho(NH_2)$ IR mode frequencies and (b) FWHM values for DMMn: 3.1% $Cr^{3+}$ (circles) and DMMn (triangles). Solid lines are to guide the eye.

The presented data show that changes in the Raman and IR spectra of DMMn: 3.1% $Cr^{3+}$ are similar to those observed for undoped DMMn. This behavior proves that similar as in DMMn, the structural changes in DMMn: 3.1% $Cr^{3+}$ can be attributed to ordering of $DMA^{+}$ cations, which is accompanied by distortion of the metal formate framework. However, closer inspection of the

data shows also some significant differences. Firstly, the observed changes in DMMn: 3.1% $Cr^{3+}$ are not so sharp as in DMMn but they are smeared over 100-160 K range. This behavior is consistent with shift of the phase transition temperature to lower value and its diffuse character. Secondly, the observed frequency shifts of the $\nu_{as}$(CNC) and $\nu_s$(CNC) modes when going from room-temperature to 5 K are smaller for DMMn: 3.1% $Cr^{3+}$ compared to DMMn. Furthermore, Figures 5 and 6 show that bands of DMMn: 3.1% $Cr^{3+}$ are broader and splitting smaller when compared to DMMn. This behavior points to weaker distortion of the framework and smaller changes in the C-N bond lengths at $T_c$ upon doping this MOF with chromium ions.

**Optical Studies of DMMn: 3.1 % $Cr^{3+}$**

Emission measured at 250 K is broad, centered at 12909 $cm^{-1}$ (787.6 nm) and its FWHM is equal 2841 $cm^{-1}$ (Figure 9). This broad band can be assigned to the $^4T_{2g} \rightarrow {}^4A_{2g}$ transition of $Cr^{3+}$. Additional small peak at 14553 $cm^{-1}$ (686.5 nm) is due to the $^2E_g \rightarrow {}^4A_{2g}$ spin forbidden transition commonly known as R line. Other humps at 14138 $cm^{-1}$ (707.9 nm) and 14286 $cm^{-1}$ (700 nm) can be assigned to vibronic transitions associated with the R line. The broad band is symmetrical, which indicates that the chromium ions are located at one site in the structure.

Figure 9. Emission spectra of DMMn: 3.1% $Cr^{3+}$ recorded at 5 - 250 K under 450 nm laser diode excitation.

With decreasing temperature the $^4T_{2g} \rightarrow {}^4A_{2g}$ transition becomes less visible. At 100 K it is no longer observed, only the peaks associated with the $^2E_g \rightarrow {}^4A_{2g}$ transition are present in the spectrum. This behavior is common for $Cr^{3+}$ ions in the intermediate crystal field.[28,29] Measurement at 5 K helped to explain the nature of narrow peaks that appear at longer wavelengths. Energies and tentative assignment of these peaks are collected in Table S2. The R lines have their maximum values at 14635.9 $cm^{-1}$ (683.2 nm) and 14593.9 $cm^{-1}$ (685.2 nm). The separation between $R_1$ and $R_2$ lines is 42 $cm^{-1}$, which is close to the 48.8 $cm^{-1}$ value found in $[(CH_3)_2NH_2][Na_{0.5}Cr_{0.5}(HCOO)_3]$.[18] This result indicates that symmetry of $Cr^{3+}$ ions surrounding in DMMn: 3.1 % $Cr^{3+}$ is similar to that in $[(CH_3)_2NH_2][Na_{0.5}Cr_{0.5}(HCOO)_3]$. This result is consistent with octahedral coordination of $Cr^{3+}$ ions due to formation of Cr-O bonds with oxygen atoms of the formate groups. Since the lifetimes of all lines are the same, we conclude, that the $Cr^{3+}$ pair lines are not present in the spectrum. Hence, all of the other lines besides R lines must be assigned to vibronic transitions. The intensity ratio of emission lines changes significantly with decreasing temperature. Lines assigned to vibronic Stokes transitions have significantly lower intensity at low temperature.

Excitation spectrum recorded at 77 K is also characteristic for $Cr^{3+}$ ions located at intermediate ligand field (Figure S11). Two broad bands centered at 17300 and 24456 $cm^{-1}$ were assigned according to $O_h$ notation to the transitions from the ground $^4A_{2g}$ to the $^4T_{2g}$ and $^4T_{1g}$(F) levels, respectively. The bands are broadened and especially the latter one is split into two components centered at 24440 and 26875 $cm^{-1}$, which is due to the fact that the degeneracy of the energy levels is removed by lower than $O_h$ symmetry. The splitting is relatively large (2435 $cm^{-1}$)

when compared to the splitting of the $^4T_{1g}$ band in $ZnAl_2O_4:Cr^{3+}$ (1860 $cm^{-1}$) or natural $MgAl_2O_4:Cr^{3+}$ (1700 $cm^{-1}$) spinels.[28,30] It is, however, comparable to the 2500 $cm^{-1}$ value observed in the synthetic $MgAl_2O_4$,[28] and smaller than the 2914 $cm^{-1}$ splitting found in $[(CH_3)_2NH_2][Na_{0.5}Cr_{0.5}(HCOO)_3]$.[18]

We have used the excitation spectrum for calculation of the crystal field parameter Dq and Racah parameters B and C. Value of the B parameter was found computing when the determinant (where: $T_F$ is energy of the $^4T_1(F)$ band) defined below is equal 0.

$$\begin{vmatrix} 10Dq + 12B - T_F & 6B \\ 6B & 20Dq + 3B - T_F \end{vmatrix} \quad (1)$$

C parameter was calculated from:

$$C = E_g + 1.8\frac{B^2}{Dq} - 7.9B \quad (2)$$

The calculated values are Dq=1730 $cm^{-1}$, B=722 $cm^{-1}$, C=3107 $cm^{-1}$, thus the ratio Dq/B=2.4 and C/B=4.3. On the basis of Tanabe – Sugano description, which was discussed in our previous paper on $[(CH_3)_2NH_2][Na_{0.5}Cr_{0.5}(HCOO)_3]$,[18] we confirm that the changes of emission spectrum with temperature result from intermediate field of ligands surrounding chromium ions.

Measurements of the emission decay profiles shown in Figure S12 also confirm the foregoing findings. The decay profiles of the R line measured in temperature range of 5 - 300 K are single exponential. From 5 to 100 K emission lifetime is constant (1.81 ms). Emission lifetime begins to decrease exponentially with temperature above 100 K, reaching 0.17 µs at 300 K. The shortening of the emission lifetime can be attributed to thermalization of the $^2E_g$ level and

energy transfer to the $^4T_{2g}$ level. This mechanism was covered in our paper on $[(CH_3)_2NH_2][Na_{0.5}Cr_{0.5}(HCOO)_3]$.[18] However, the energy separation is greater in DMMn: 3.1 $Cr^{3+}$ when compared to $[(CH_3)_2NH_2][Na_{0.5}Cr_{0.5}(HCOO)_3]$ because the chromium ions are located in a slightly stronger ligand field. This result indicates that Cr-O bonds in DMMn: 3.1 $Cr^{3+}$ should be slightly shorter when compared to Cr-O bonds in $[(CH_3)_2NH_2][Na_{0.5}Cr_{0.5}(HCOO)_3]$.

To establish the value of the $^2E_g$ - $^4T_{2g}$ separation ΔE (see Figure S13), following procedure was carried out. According to Grinberg et al. the probability of radiative transition in $Cr^{3+}$ can be expressed as:[31]

$$P(T) = \frac{P_{^2E_g} + N_{^2T_1} P_{^2T_1} \exp\left(-\frac{\Delta E_1}{kT}\right) + N_{^4T_2} P_{^4T_2} \exp\left(-\frac{\Delta E}{kT}\right)}{1 + N_{^2T_1} \exp\left(-\frac{\Delta E_1}{kT}\right) + N_{^4T_2} \exp\left(-\frac{\Delta E}{kT}\right)} \quad (3)$$

where P and N are the transition probabilities and degeneracies of excited states, respectively. ΔE and $\Delta E_1$ are the energy separations between $^2E$ - $^4T_2$ and $^2T_1$ - $^2E$, respectively. Taking into consideration only $^2E_g$ and $^4T_{2g}$, the formula simplifies to:

$$P(T) = \frac{P_{^2E_g} + N_{^4T_2} P_{^4T_2} \exp\left(-\frac{\Delta E}{kT}\right)}{1 + N_{^4T_2} \exp\left(-\frac{\Delta E}{kT}\right)} \quad (4)$$

The result of fitting the experimental data to Eq. (4) are shown in Figure 10. The value of the $^2E_g$ - $^4T_{2g}$ separation is calculated to be 1442 ± 49 $cm^{-1}$. This value is comparable with results for $Cr^{3+}$ in intermediate ligand field in spinels.[28] By comparison of the obtained ΔE with the values for spinels and corresponding Dq/B values, we can see that for the ΔE = 1442 $cm^{-1}$, the Dq/B value should be between 2.3 - 2.4. This conclusion is in agreement with the value calculated from the spectra.

Figure 10. Emission lifetimes recorded at 5 – 300 K temperature range. Solid line represents fitted curve (2) with parameters: $\tau_0$ = 1.75 ± 0.08 ms, $\tau_2$ = 0 ± 32ns, $N_2$ = 1, $\Delta E$ = 1442 ± 49 $cm^{-1}$. Adj. R-Square for fitting is 0.99862.

**Optical Studies of DMMn: 1.4 % $Eu^{3+}$ and DMMn: 2.6 % $Er^{3+}$**

Figure S14 shows absorption spectra of europium- and erbium-doped DMMn. As can be seen, the absorption bands characteristic for $Er^{3+}$ and $Eu^{3+}$ are clearly observed, proving incorporation of these ions into the manganese formate framework.

Figure 11 shows emission spectrum of DMMn: $Eu^{3+}$ measured at 77 K. The $^5D_0 \rightarrow {}^7F_2$ electric dipole transition dominates the emission spectrum. The second strongest transition is the $^5D_0 \rightarrow {}^7F_4$ one. Transitions to the $^7F_3$, $^7F_5$, and $^7F_6$ manifolds are much weaker. The $^5D_0 \rightarrow {}^7F_1$ transition gains its strengths because of magnetic–dipole character and the $^5D_0 \rightarrow {}^7F_0$ one is very weak. It is well known that emission spectra may provide information on the symmetry of the first coordination sphere of this ion since the number of crystal-field components for the $^5D_0 \rightarrow {}^7F_j$ transitions as well as intensity of observed emission lines depend on the site symmetry of $Eu^{3+}$ ions.[32] For instance, strong intensity of $^5D_0 \rightarrow {}^7F_2$ transition indicates that $Eu^{3+}$ ions are located at low symmetry noncentrosymmetric sites with highly polarizable ligands.[32] The presence of strong

$^5D_0 \rightarrow {}^7F_2$ emission and splitting of the emission bands for DMMn: 1.4 % $Eu^{3+}$ samples is characteristic for $Eu^{3+}$ ions located at low symmetry site and coordination to carboxylate groups.



Figure 11. 1Emission spectrum of DMMn: 1.4 % $Eu^{3+}$ recorded at 77 K, $\lambda_{exc}$= 396 nm.

The above examples show that both $Eu^{3+}$ and $Er^{3+}$ ions may be incorporated into DMMn host matrix. Luminescent lanthanide-based MOFs with small concentration of lanthanide ions are still scarce. One of a possible way for designing such MOFs is synthesis of heterometallic frameworks.[33] One of the example is $[Zn_5Eu(OH)(H_2O)_3(mip)_6 \cdot (H_2O)]_n$ and its Tb analogue (mip= 5-methylisophthalate dianion).[34] Another way for obtaining lanthanide-doped MOFs is cation-exchange. This method was, for instance, employed for synthesis of lanthanide-doped $[NH_4]_2[ZnL]\cdot 6H_2O$, where L=1,2,4,5-benzenetetracarboxylate.[35] The third method is a direct synthesis of lanthanide-doped MOFs.[36] *In situ* doping of low concentration of lanthanide ions is especially promising way for obtaining efficient luminescent materials due to avoiding luminescent quenching and simultaneously maintaining the main properties of the host matrix.[36] However, there are still very few reports on synthesis of lanthanide-doped MOFs using this *in situ* method. Our results show new way for growing DMMn and related MOFs doped with lanthanide ions.

## Conclusions

We have demonstrated that some amine-templated metal formates belonging to the large family of multiferroic MOFs may be doped by various trivalent cations. This doping leads to shift of $T_c$ to lower value. The doping also changes the phase transition character from a strongly first-order into diffused one due to compositional fluctuations within the sample. Detailed investigation of DMMn: 3.1 % $Cr^{3+}$ sample shows, however, that the structural changes in the this sample are still very similar to those observed for undoped DMMn. Thus the doped samples are still expected to exhibit multiferroic properties, at least if the concentration of the dopant ions is within a few percentage range. However, the doping should affect value of the spontaneous polarization as well as the coupling strength between magnetic and electric orders. Our results also show that it affects the dielectric relaxation processes.

Another interesting result of our study is manifestation of luminescence of $Cr^{3+}$ and $Eu^{3+}$ ions doped into DMMn host. This discovery shows that doping may add new functionality to this family of multiferroic MOFs, i.e., chromium- and lanthanide-doped samples may exhibit luminescent properties. Luminescent MOFs are of great interest for various technological applications such as sensors and solid-state lightning devices, among others, and a number of luminescent MOFs are already known. However, chromium-based MOFs are still very scarce. There are also few examples of MOFs containing low concentration of lanthanide ions but such materials are of great interest since low concentration of dopant ions helps to avoid luminescence quenching. Furthermore, modification of the lanthanide ions concentration is one of very important strategy for tuning luminescent properties in solids. For instance, Liu *et al.* showed that changes of $Eu^{3+}$ concentration in $Tb(1,3,5\text{-BTc})(H_2O)_3{\cdot}3H_2O$: $Eu^{3+}$ allows tuning luminescent

color from green to yellow, orange and red-orange.[37] Thus our discovery showing that some multiferroic MOFs may be doped with $Cr^{3+}$ and lanthanide ions opens up a fascinating opportunity for synthesis of various multifunctional amine-templated metal formate frameworks with tunable multiferroic and luminescent properties by doping trivalent cations into these frameworks. We would like to emphasize that although perovskite-type organic-inorganic hybrid ferroelectrics and luminescent ferroelectrics are known (examples are $[C_5H_9\text{-}NH_3][CdCl_3]$ and (pyrrolidinium$MnCl_3$),[38,39] discovery of the first luminescent multiferroic MOF (pyrrolidinium$MnBr_3$) was reported just a few months ago.[40] Thus the synthesised here chromium-doped multiferroic DMMn and DMCo as well as europium-doped DMMn constitute the first luminescent multiferroic materials based on chromium and lanthanide ions.

**Acknowledgements**

This research was supported by the National Center for Science (NCN) in Poland under project No. DEC-2013/11/B/ST5/01058.

## Notes

[a]Institute of Low Temperature and Structure Research, Polish Academy of Sciences, Box 1410, 50-950 Wrocław 2, Poland; m.maczka@int.pan.wroc.pl; phone: +48-713954161; fax: +48-713441029

[b]Faculty of Fundamental Problems of Technology, Wrocław University of Technology, Wybrzeże Wyspiańskiego 27, 50-370 Wrocław, Poland

Electronic Supplementary Information (ESI) available: Figures S1-S14: Powder X-ray diffraction, DSC traces, IR and Raman spectra, temperature dependence of bandwidths and frequencies, excitation and absorption spectra, emission decay profiles and single configurational coordinate model for $Cr^{3+}$ in intermediate ligand field. Tables S1 and S2: values of phase transition temperatures and associated changes in enthalpy and entropy as well as emission peaks at 5 K and their assignment.

## References

1 U. Böttger, in "Polar Oxides, Properties, Characterization and Imaging", Ed. R. Waser, U. Böttger, S. Tiedke, Wiley-VCH, Weinheim 2005.

2 J. Kreisel, B. Noheda and B. Dkhil, *Phase Trans.* 2009, **82,** 633-661.

3 K. F. Wang, J.-M. Liu and Z. F. Ren, *Adv. Phys*. 2009, **58,** 321-448.

4 (a) P. Jain, V. Ramachandran, R. J. Clark, H. D. Zhou, B. H. Toby, N. S. Dalal and H. W. Kroto, A. K. J. Cheetham, *J. Am. Chem. Soc*., 2009, **131**, 13625-13627. (b) G. Rogez, N. Viart and M. Drillon, *Angew. Chem. Int. Ed.* 2010, **49,** 1921-1923.

5 (a) D. W. Fu, W. Zhang, H. L. Cai, Y. Zhang, J. Z. Ge, R. G. Xiong, S. D. Huang and T. Nakamura, *Angew. Chem. Int. Ed*., 2011, **50**, 11947-11951. (b) Y. Tian, J. Cong, S. Shen, Y. Chai, L. Yan, S. Wang and Y. Sun, *Phys. Stat. Sol. RRL* 2014, **8,** 91-94. (c) Y. Tian, A. Stroppa, Y. Chai, L. Yan, S. Wang, P. Barone, S. Picozzi and Y. Sun, *Sci. Rep.* 2014, **4,** 6062.

6 G. C. Xu, W. Zhang, X. M. Ma, Y. H. Hen, L. Zhang, H. L. Cai, Z. M. Wang, R. G. Xiong and S. Gao, *J. Am. Chem. Soc*., 2011, **133**, 14948-14951.

7 (a) B. Pato Dolán, L. C. Gómez-Aguirre, J. M. Bermúdes-García, M. Sánchez-Andújar, A. Fondado, J. Mira, S. Castro-Garcia and M. A. Señaris-Rodriguez, *RSC Advances* 2013, **3,** 22404-22411. (b) S. Chen, R. Shang, K.-L. Hu, Z.-M. Wang and S. Gao, *Inorg. Chem. Front***. 2014, 1,**

83-98. (c) A. Stroppa, P. Jain, P. Barone, M. Marsman, J. M. Perez Mato, A. K. Cheetham, H. W. Kroto and S. Picozzi, *Angew. Chem. Int. Ed*. 2011, **50,** 5847-5850. (d) D. Di Sante, A. Stroppa, P. Jain and S. Picozzi, *J. Am. Chem. Soc*. 2013, **135,** 18126-18130. (e) R. Shang, G. C. Xu, Z. M. Wang and S. Gao, *Chem. Eur. J*. 2014, **20,** 1146-1158.

8 W. Wang, L.-Q. Yan, J.-Z. Cong, Y.-L. Zhao, F. Wang, S.-P. Shen, T. Zhou, D. Zhang, S.-G. Wang, X.-F. Han and Y. Sun, *Sci. Rep*. 2013, **3,** 2024.

9 (a) B. Zhou, Y. Imai, A. Kobayashi, Z. M. Wang and H. Kobayashi, *Angew. Chem. Int. Ed*. 2011, **50,** 11441-11445. (b) Y. Imai, B Zhou, Y. Ito, H. Fijimori, A. Kobayashi, Z. M. Wang and H. Kobayashi, *Chem. Asian J.* 2012, **7,** 2786-2790. (c) M. Mączka, T. A. Da Silva, W. Paraguassu, M. Ptak and K. Hermanowicz, *Inorg. Chem*. 2014, **53,** 12650-12657.

10 B. Liu, R. Shang, K.-L. Hu, Z.-M. Wang and S. Gao, S. *Inorg. Chem.* 2012**, 51,** 13363-13372.

11 M. Mączka, A. Ciupa, A. Gągor, A. Sieradzki, A. Pikul, B. Macalik and M. Drozd, *Inorg. Chem*., 2014, **53**, 5260-5268.

12 (a) A. Rossin, M. R. Chierotti, G. Giambiastiani, R. Gobetto and M. Peruzzini, *Cryst. Eng. Comm*., 2012, **14**, 4454-4460. (b) A. Ciupa, M. Mączka, A. Gągor, A. Pikul, E. Kucharska, J. Hanuza and A. Sieradzki, *Polyhedron* 2015, **85,** 137-143.

13 (a) K. S. Hagen, S. G. Naik, B. H. Huynh, A. Masello and G. Christou, *J. Am. Chem. Soc*., 2009, **131**, 7516-7517. (b) J.-P. Zhao, B.-W. Hu, F. Lloret, J. Tao, Q. Yang, X.-F. Zhang and X.-H. Bu, *Inorg. Chem*., 2010, **49**, 10390-10399.

14 L. Cañadillas-Delgado, O. Fabelo, J. A. Rodríguez-Velamazán, M.-H. Lemėe-Cailleau, S. A. Mason, E. Pardo, F. Lloret, J.-P. Zhao, X.-H. Bu, V. Simonet, C. V. Colin and J. Rodríguez-Carvajal, *J. Am. Chem. Soc*., 2012, **134**, 19772-19781.

15 A. Ciupa, M. Mączka, A. Gągor, A. Sieradzki, J. Trzmiel, A. Pikul and M. Ptak, *Dalton Trans.*, 2015, **44,** 8846-8854.

16 A. Ciupa, M. Mączka, A. Gągor, A. Pikul and M. Ptak, *Dalton Trans.* 2015, **44,** 13234-13241.

17 M. Mączka, A. Pietraszko, L. Macalik, A. Sieradzki, J. Trzmiel and A. Pikul, *Dalton Trans.* 2014, **43,** 17075-17084.

18 M. Mączka, B. Bondzior, P. Dereń, A. Sieradzki, J. Trzmiel, A. Pietraszko and J. Hanuza, *Dalton Trans.*, 2015, **44,** 6871-6879.

19 M. Sánchez-Andújar, S. Presedo, S. Yáñez-Vilar, S. Castro-García, J. Shamir and M. A. Señaris-Rodriguez, *Inorg. Chem.* 2010, **49,** 1510-1516.

20 M. Mączka, A. Gągor, B. Macalik, A. Pikul, M. Ptak and J. Hanuza, *Inorg. Chem*., 2014, **53**, 457-467.

21 B. Pato Dolán, M. Sánchez-Andújar, L. C. Gómez-Aguirre, S. Yáñez-Vilar, J. Lopez-Beceiro, C. Gracia-Fernandez, A. A. Haghighirad, F. Ritter, S. Castro-Garcia and M. A. Señaris-Rodriguez, *Phys. Chem. Chem. Phys*., 2012, **14**, 8498-8501.

22 K. Vinod, C. S. Deepak, S. Sharma, D. Sornadurai, A. T. Satya, T. R. Ravindran, C. S. Sundar and A. Bharathi, *RSC Adv.* 2015, **5,** 38818-37822.

23 M. Guo, H. L. Cai and R. G. Xiong, *Inorg. Chem. Commun*., 2010, **13**, 1590-1598.

24 D. Rout, V. Subramanian, K. Hariharan and V. Sivasubramanian, *Sol. State Commun.* 2006, **137,** 446-450.

25 S. Lee, C. A. Randall and Z. K. Liu, *J. Am. Ceram. Soc.* 2007, **90,** 2589-2594.

26 C. Carabatos-Nedelec and P. Becker, *J. Raman Spectrosc*. 1997, **28,** 663-671.

(27) M. Maczka, A. G. Souza Filho, W. Paraguassu, P. T. C. Freire, J. Mendes Filho and J. Hanuza, *Prog. Mater. Sci*. 2012, **57,** 1335-1381.

28 P. J. Dereń, M. Malinowski and W. Stręk, *J. Luminesc.* 1996, **68,** 91-103.

29 P. J. Dereń, A. Watras, A. Gągor and R. Pązik, R. *Cryst. Growth Des.* 2012, **12,** 4752-4757.

30 J. Derkosch, W. Mikenda and A. Preisinger, *J. Sol. State Chem*. 1977, **22,** 127-133.

31 M. Grinberg, *J. Luminesc.* 1993, **54,** 369-382.

32 K. Binnemans, *Coord. Chem. Rev*. 2015, **295,** 1-45.

33 L. V. Meyer, F. Schönfeld and K. Müller-Buschbaum, *Chem. Commun*. 2014, **50,** 8093-80108.

34 Q.-B. Bo, H.-Y. Wang, D.-Q. Wang, Z.-W. Zhan, J.-L. Miao and G.-X. Sun, *Inorg. Chem.* 2011, **50,** 10163-10177.

35 F. Luo and S. R. Batten, *Dalton Trans.* 2010, **39,** 4485-4488.

36 N. T. Binh, D. M. Tien, L. T. K. Giang, H. T. Khuyen, N. T. Huong, T. T. Huong and T. D. Lam, *Mat. Chem. Phys*. 2014, **143,** 946-951.

37 K. Liu, H. You, Y. Zheng, G. Jia, Y. Song, Y. Huang, M. Yang, J. Jia, N. Guo and H. Zhang, *J. Mater. Chem.* 2010, **20,** 3272-3279.

38 Y. Zhang, H.-Y. Ye, W. Zhang and R.-G. Xiong, *Inorg. Chem. Front.* 2014, **1,** 118-123.

39 Y. Zhang, W.-Q. Liao, D.-W. Fu, H.-Y. Ye, Z.-N. Chen and R.-G. Xiong, *J. Am. Chem. Soc.* 2015, **137,** 4928-4931.

40 Y. Zhang, W.-Q. Liao, D.-W. Fu, H.-Y. Ye, C.-M. Liu, Z.-N. Chen and R.-G. Xiong, *Adv. Mater.* 2015, **27,** 3942-3946.

We show that doping of multiferroic formates with various trivalent cations is a new route for synthesis of tunable luminescent multiferroics

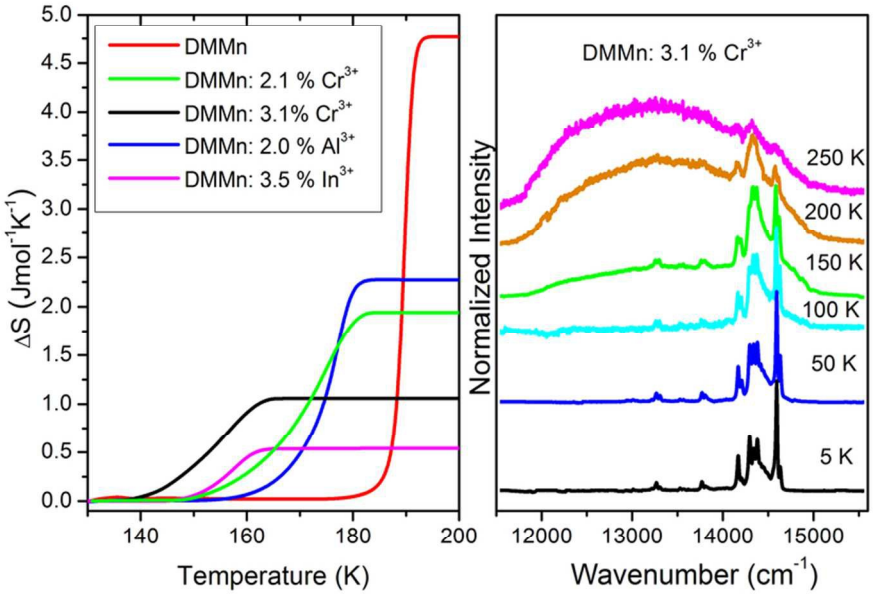


39x28mm (600 x 600 DPI)